Journal of Materials Chemistry C

ROYAL SOCIETY OF CHEMISTRY

PAPER

View Article Online
View Journal | View Issue

Cite this: J. Mater. Chem. C, 2022, 10, 4775

Bridge control of photophysical properties in benzothiazole-phenoxazine emitters – from thermally activated delayed fluorescence to room temperature phosphorescence†

Simon Paredis,[ab] Tom Cardeynaels,[abc] Jasper Deckers,[ab] Andrew Danos,[d] Dirk Vanderzande,[ab] Andrew P. Monkman,[d] Benoît Champagne[c] and Wouter Maes*[ab]

Received 12th October 2021,
Accepted 4th January 2022

DOI: 10.1039/d1tc04885f

rsc.li/materials-c

The bridging phenyl group in a fluorescent phenoxazine-benzothiazole donor–acceptor dyad is replaced by either a naphthalene or a thiophene moiety to probe the influence of a more extended conjugated system or the presence of a sulfur-containing heteroaromatic spacer on the emissive properties. These seemingly small structural alterations strongly affect the relative positions of the excited states, the fluorescence intensity, and the emission mechanism. Consequently, thermally activated delayed fluorescence (TADF) is observed at longer timescales for the materials with phenyl and naphthalene linkers, whereas the thiophene group promotes room temperature phosphorescence (RTP), both in the solid state and in solution, and enhances singlet oxygen generation. Phosphorescence in solution at ambient temperature from a purely organic molecule without heavy halogen functionalisation is quite rare, and this unique property calls for further specific attention.

Introduction

Purely organic molecules that emit light upon applying an electric current are highly attractive because of their strong potential for organic light-emitting diodes (OLEDs).[1,2] These electroluminescent properties arise from the radiative decay of excitons,[3] which are electrically generated in an excited singlet or triplet state with a statistical probability of 25 and 75%, respectively.[4,5] The transition from the first singlet excited state to the ground state ($S_1 \rightarrow S_0$, *i.e.* fluorescence) represents an exchange between two electronic states with identical spin multiplicity and as such is a spin-allowed transition,[6] generally with a lifetime in the nanoseconds regime. On the other hand, the transition from the first triplet excited state to the ground state ($T_1 \rightarrow S_0$, *i.e.* phosphorescence) occurs between two electronic states with different spin multiplicity and is therefore a spin-forbidden and considerably slower transition (typically in the order of microseconds).[6,7]

While the second generation OLED devices are able to harvest triplet excitons by spin–orbit coupling (SOC) enhanced phosphorescence from heavy metal complexes, the third generation focusses on triplet up-conversion strategies to achieve near-unity internal quantum efficiency and singlet emission. There are three leading mechanisms for the indirect generation and emission of singlet excited states, *i.e.* thermally activated delayed fluorescence (TADF), hybridised local and charge-transfer (HLCT) emission, and triplet–triplet annihilation (TTA).[8] TADF is the most promising emission mechanism for highly efficient exciton harvesting and it has become a very popular strategy to enhance OLED efficiency in recent years.[9,10] For TADF to occur, the first excited singlet state and the first two excited triplet states, which are mixed by vibronic coupling, should be in close proximity (<200 meV).[11] This small energy difference enables transitions between the relevant excited states ($S_1 \rightleftarrows T_{1,2}$). Consequently, if the transition rate from the triplet excited state to the singlet excited state, *i.e.* reverse intersystem crossing (rISC), is higher than other (non)radiative pathways from the triplet states, the singlet excited state will be (re)populated.[12] As a result, a delayed emission occurs from the singlet excited state, with the same energy as regular fluorescence. Since the delayed fluorescence relies on slow rISC from

[a] Hasselt University, Institute for Materials Research (IMO-IMOMEC), Design & Synthesis of Organic Semiconductors (DSOS), Agoralaan 1, 3590 Diepenbeek, Belgium. E-mail: wouter.maes@uhasselt.be
[b] IMOMEC Division, IMEC, Wetenschapspark 1, 3590 Diepenbeek, Belgium
[c] University of Namur, Laboratory of Theoretical Chemistry, Theoretical and Structural Physical Chemistry Unit, Namur Institute of Structured Matter, Rue de Bruxelles 61, 5000 Namur, Belgium
[d] OEM group, Department of Physics, Durham University, South Road, Durham DH1 3LE, UK

† Electronic supplementary information (ESI) available. See DOI: 10.1039/d1tc04885f

triplet states, it occurs with lifetimes in the microseconds regime. TADF emitters can thus harvest excitons from both the singlet and triplet states, affording highly efficient light-emitting devices.[13]

Organic molecules exhibiting TADF generally consist of a combination of an electron-donating (D) and an electron-accepting (A) part. While the size of the singlet–triplet splitting is largely determined by the frontier molecular orbital overlap, the rational design of a D–A or push–pull dyad showing TADF remains challenging because of the complex interplay between the excited state energy levels.[14] As a result, other phenomena such as room temperature phosphorescence (RTP) are sometimes observed in molecules designed to show TADF emission. It is only in recent years that purely organic RTP, not relying on the SOC of metallic ions in organometallic phosphors, has risen to prominence.[15–17] Besides the need for sufficient SOC, a second criterion for RTP needs to be met, *i.e.* the suppression of non-radiative transitions caused by vibrational losses and collisions. This collisional quenching can be reduced by fixing the emitting molecules in a solid-state environment, as is typically done for OLEDs. On the other hand, RTP in solution has been rarely observed due to the high molecular mobility in a solvent medium, favouring non-radiative transitions.[18,19]

While a large number of TADF emitters can be found in the literature, and many make use of a π-bridge between the donor and acceptor parts of the molecule, only a few reports exist about the influence of this π-bridge on the photophysical properties of a given molecule and whether or not the π-bridge can be used to tune the emissive properties of the fluorophore. It has been illustrated that the introduction of such π-bridges,[20,21] and the addition of substituents such as methyl,[22] trifluoromethyl,[23] nitrile,[24] or extra phenyl groups[21,25–27] onto these bridges, has a great impact on the emissive properties (*e.g.* colour, quantum yield, rate of (r)ISC) by restricting the rotational freedom, altering the acceptor strength, and/or increasing the space between donor and acceptor. In this work, 10-(4-(benzo[*d*]thiazol-2-yl)phenyl)-10*H*-phenoxazine (**BTaz-Ph-PXZ**; Scheme 1), a fluorescent molecule already reported to show green TADF emission by Adachi *et al.*,[28] is used as a suitable scaffold to perform such an investigation. The bridging phenyl moiety is systematically replaced by either a naphthalene (**BTaz-Na-PXZ**) or a thiophene unit (**BTaz-Th-PXZ**). We find that by altering the bridging unit, the energy of the excited triplet states changes, while keeping the excited singlet state energies relatively similar. Consequently, these dyads all have the same emission colour, but the emission mechanisms and their efficiencies are very different, controlled by the bridge. These emission kinetics and mechanisms are elucidated from (time-resolved) photophysical measurements in solution and in film, and corroborated by dedicated quantum-chemical calculations.

Results and discussion

Benzothiazole (BTaz) is used here as a small acceptor molecule, which has already shown great potential in other fields of organic electronics such as organic photovoltaics (OPVs),[29] organic field-effect transistors (OFETs),[30,31] and OLEDs.[32] This acceptor unit is combined with phenoxazine (PXZ), a strong donor moiety commonly used in the field of TADF as it tends to give rise to stable high-energy triplet states and it has a large dihedral angle with adjacent groups.[33–35] To finalise the design, a phenyl,[28] naphthyl, or thienyl group is introduced as a π-bridge between the donor and the acceptor to obtain a clear separation of the highest occupied and lowest unoccupied molecular orbital (HOMO and LUMO, respectively). The starting

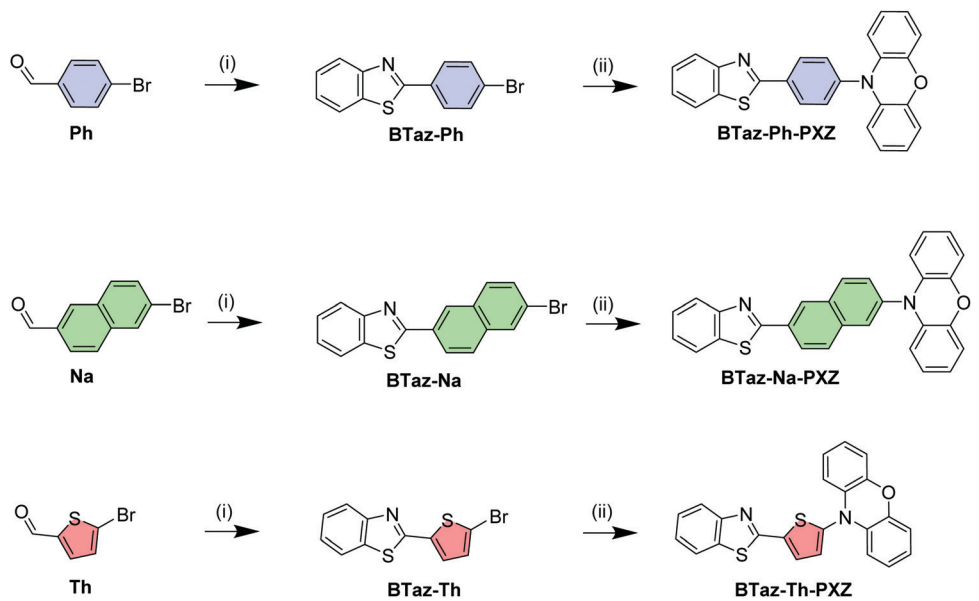

Scheme 1 Synthesis procedures for the three **BTaz-Ar-PXZ** emitters: (i) 2-aminothiophenol, sodium metabisulfite, DMF, reflux, 2 h; (ii) $Pd(OAc)_2$, 10*H*-phenoxazine, $(t\text{-Bu})_3P$, NatBuO, toluene, reflux, 16 h.

materials for the dyad synthesis are the three respective aromatic bridge molecules substituted with a bromine and an aldehyde group on the appropriate positions. First, the aldehyde functionality was reacted with 2-aminothiophenol in the presence of sodium metabisulfite, a nontoxic inorganic oxidant,[36] to yield the benzothiazole unit. Afterwards, a Buchwald–Hartwig cross-coupling reaction was performed to attach the phenoxazine unit, affording **BTaz-Ph-PXZ**, **BTaz-Na-PXZ**, and **BTaz-Th-PXZ** (Scheme 1). Details on the synthesis procedures and characterization data are provided in the ESI.†

The geometries of the three D–A chromophores were optimised using density functional theory (DFT) calculations with M06/6-311G(d).[37] Time dependent DFT (TDDFT) calculations were additionally performed to estimate the singlet and triplet energies using a modified LC-BLYP (ω = 0.17 bohr^{-1}) exchange correlation (XC) functional, which is optimised for TADF research,[38,39] with the Tamm–Dancoff approximation (TDA) and the 6-311G(d) basis set. TDDFT calculations were done using the polarizable continuum model (PCM) in cyclohexane to simulate a non-polar environment. The orbital spatial distributions were obtained from single-point calculations that are performed during the TDDFT calculations and are hence obtained using the same LC-BLYP/6-311G(d) method. All calculations were performed using the Gaussian16 package.[40] The charge-transfer (CT) character of the involved states was investigated by looking at the differences of ground and excited state electron densities. These were characterised by the distance over which the electronic charge is transferred (d_{CT}) and the related change in dipole moment ($\Delta\mu$), which were calculated according to the work of Le Bahers and coworkers.[41] The PySOC program was used to calculate the SOC values using the same XC functional, basis set, and PCM treatment as for the TDDFT calculations.[42]

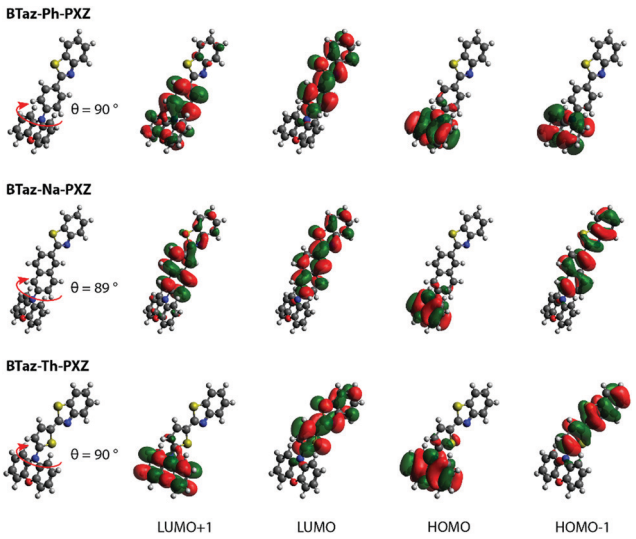

Fig. 1 HOMO–LUMO spatial distributions for **BTaz-Ph-PXZ**, **BTaz-Na-PXZ**, and **BTaz-Th-PXZ**. Isocontour values of 0.02 (a.u.) were used for all orbitals.

DFT geometry optimizations illustrated that the PXZ moiety is nearly perpendicular (*i.e.* ±90° torsion angle) with respect to the aromatic unit linking PXZ and BTaz, as shown in Fig. 1. Moreover, the bridging unit is in all cases coplanar with the benzothiazole group, making it electronically a part of the acceptor rather than a simple non-interacting bridge. The optimised geometries and the corresponding HOMO and LUMO spatial distributions reveal that the HOMO is (mostly) located on the PXZ moiety, while the LUMO is spread over the BTaz-Ar unit, resulting in well-separated HOMO–LUMO topologies and suggesting strong CT character of the lowest-energy excited singlet state. This CT nature is also visualised in Fig. S1 (ESI†), where the difference in electron density between the ground and (different) excited states is shown. A clear CT character is observed in the first singlet and the first triplet for **BTaz-Ph-PXZ**, while the second singlet state seems to show some CT character from the PXZ donor unit to the phenyl bridge. CT character is also observed in the first and second singlet and the second triplet state in the case of **BTaz-Na-PXZ**, and in the first singlet and second triplet state for **BTaz-Th-PXZ**. The calculated excitation energies for the most relevant excited states are listed in Table 1. The first two excited triplet states are close in energy to the first excited singlet state, potentially allowing TADF. Furthermore, for the three compounds, the dominant HOMO–LUMO nature of the vertical transition towards the first excited singlet state, together with the CT distance and the change in dipole moment (listed in Table 2), demonstrates the substantial CT character. For other relevant excited states, the nature of the transitions is not always from HOMO to LUMO, leading to more localised excitonic states and smaller values for both d_{CT} and $\Delta\mu$ (Table 2). The distributions of the other molecular orbitals taking part in these transitions (*i.e.* HOMO−1 and LUMO+1) are shown in Fig. 1. UV-Vis absorption spectra were simulated (Fig. S2, ESI†) and are dominated by a band at higher energy than the aforementioned CT states, which often have negligible absorption cross-section. A dihedral angle of 10° was considered to account for the vibrational freedom of the PXZ moiety with respect to the rest of the molecule.

To better understand which states are dominating the UV-vis absorption spectra, the TDDFT investigation was expanded to the 5th excited singlet. The higher singlet excited states (*i.e.* S_3–S_5) show localised character on different parts of the molecule depending on the excited state and the π-bridge (Fig. S1 and Table S2, ESI†). For S_3, the excited state is localised on the Ar-PXZ

Table 1 TDDFT results for the vertical first and second singlet excitation energies and the corresponding oscillator strengths (*f*), and the first and second vertical triplet excitation energies, as determined with TDDFT-TDA and a modified LC-BLYP (ω = 0.17 bohr^{-1}) exchange correlation functional

Compound	S_1 (eV)	f_{S_1}	S_2 (eV)	f_{S_2}	T_1 (eV)	T_2 (eV)	$\Delta E_{S_1-T_1}$ (eV)	$\Delta E_{S_1-T_2}$ (eV)
BTaz-Ph-PXZ	2.96	<0.001	3.56	<0.001	2.94	3.04	0.02	−0.08
BTaz-Na-PXZ	2.97	<0.001	3.56	0.001	2.81	2.90	0.16	0.07
BTaz-Th-PXZ	2.86	<0.001	3.78	0.013	2.78	2.85	0.08	0.01

Table 2 Nature of the various transitions (H = HOMO, L = LUMO), charge-transfer distance (d_{CT}), and change in dipole moment ($\Delta\mu$, excited state dipole – ground state dipole) accompanying the $S_0 \rightarrow S_x$ and $S_0 \rightarrow T_x$ (x = 1,2) transitions in cyclohexane, as determined with TDDFT-TDA and a modified LC-BLYP (ω = 0.17 bohr^{-1}) exchange correlation functional

	S_1			S_2			T_1			T_2		
Compound	Nature	d_{CT} (Å)	$\Delta\mu$ (D)	Nature	d_{CT} (Å)	$\Delta\mu$ (D)	Nature	d_{CT} (Å)	$\Delta\mu$ (D)	Nature	d_{CT} (Å)	$\Delta\mu$ (D)
BTaz-Ph-PXZ	H→L	3.79	21.42	H→L+1	1.89	6.64	H→L	3.77	20.70	H→L+1	0.17	0.39
BTaz-Na-PXZ	H→L	3.85	21.55	H→L+1	3.64	16.34	H−1→L	0.15	0.22	H→L	3.58	16.02
BTaz-Th-PXZ	H→L	3.50	19.03	H→L+1	0.54	1.49	H−1→L	0.35	0.67	H→L	3.49	18.88

part for **BTaz-Ph-PXZ** and **BTaz-Na-PXZ**, and on the BTaz-Ar part for **BTaz-Th-PXZ**, whereas the opposite is true for S_4. The 5th singlet excited state shows localization on the Ar-PXZ part for the phenyl bridged compound, whereas it is localised on the BTaz-Ar part for the naphthalene and thiophene bridged compounds. Overall, the simulated absorption profiles (Fig. S2, ESI†) are in close agreement with the experimental spectra (*vide infra*, Fig. 2).

Steady-state absorption spectra (in toluene) and both fluorescence and phosphorescence emission spectra (in zeonex film) of the three push–pull dyes are shown in Fig. 2 (and the data can be found in Table 3). For all three molecules, the absorption consists of one intense main peak and one minor peak at longer wavelength. Based on the TDDFT calculations, we can attribute the weak absorption band around 400 nm to direct CT absorption (see also Fig. S2, ESI†), whereas the intense peak around 320 nm can be attributed to locally excited (LE) singlet states. For all three compounds, the fluorescence spectra in film are very similar, while the phosphorescence peaks differ both in emission wavelength and in shape. Therefore, we can conclude that upon changing the π-bridge, the singlet excited state remains relatively unaffected, while the energy and the nature of the triplet excited state does change considerably.

The nature of the absorption and emission features of the three dyes was further analysed by solvatochromic experiments (Fig. S3 and Table S4, ESI†). Emission spectra were recorded in three different solvents, *i.e.* methylcyclohexane, toluene, and chloroform. In all three solvents, two emission peaks were observed. The lower energy emission peak shows a strong red-shift upon increasing solvent polarity, which occurs due to the stabilisation of states with CT character in more polar solvents. The solvatochromic red-shift confirms the presence of a CT state and it is therefore suggested that the structureless low energy emission peaks in toluene and chloroform originate from CT emission. The vibronic structured emission peak in methylcyclohexane on the other hand suggests emission from an LE state.

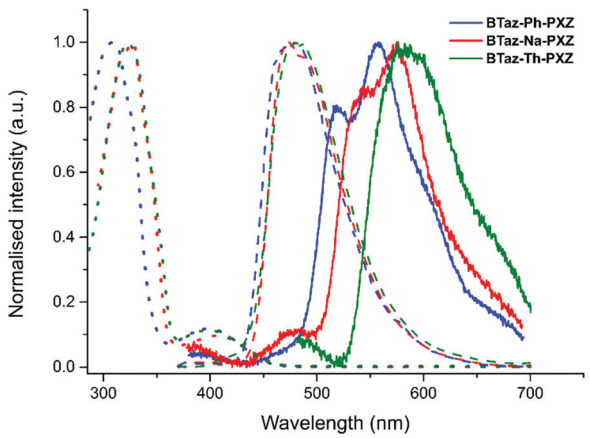

Fig. 2 Normalised steady-state absorption spectra in toluene (dotted lines), steady-state emission spectra (λ_{exc} = 355 nm) at room temperature in zeonex film (dashed lines), and time-resolved phosphorescence (λ_{exc} = 355 nm) at 80 K at a 44.7 ms decay time in zeonex film (solid lines) for **BTaz-Ph-PXZ** (blue), **BTaz-Na-PXZ** (red), and **BTaz-Th-PXZ** (green).

The higher energy emission in all three solvents shows little influence of the solvent polarity and could therefore be originating from LE states, giving rise to dual LE and CT emission. A possible explanation for this observation could be the occurrence of dual stable conformations of the PXZ donor unit with respect to the bridging moiety.[43] Relaxed potential energy surface scans were performed for all compounds (Fig. S4, ESI†), using the M06/6-311G(d) method, and the perpendicular orientation between the donor and bridge units was found to be the most stable one by more than 13 kJ mol^{-1}. This corresponds to a Boltzmann population of more than 99% for the perpendicular orientation, indicating that it is highly unlikely for the higher energy emission to be originating from a coplanar (metastable) conformer. Further investigation of the compounds in solution revealed signs of degradation under the influence of light (Fig. S5, ESI†). To verify this photodegradation, the steady-state absorption and emission of all three compounds was measured in chloroform with intermittent periods of LED (λ_{exc} = 325 nm) irradiation (Fig. S6, ESI†). It is clear that exposure to light gives rise to a relative increase in the lower energy absorption, located in the same spectral region as the CT absorption, and higher energy emission bands. This is more abundant in chloroform with respect to toluene and increases within the series from the phenyl to the thienyl spacer. These spectral changes are likely caused by photodegradation of the benzothiazole unit,[44,45] although ^{1}H NMR spectra recorded after irradiation did not show clear signs of degradation (Fig. S7, ESI†).

The fluorescence quantum yields in toluene solution and zeonex film under normal and inert atmosphere ($\Phi_{f,atm}$ and $\Phi_{f,inert}$) of all three compounds were then determined (Table 3) to gauge their luminescent properties. The results obtained for **BTaz-Ph-PXZ** are similar to the values achieved by Adachi *et al.* ($\lambda_{em,toluene}$ = 512 nm, $\Phi_{f,atm,toluene}$ = 0.17, $\Phi_{f,inert,toluene}$ = 0.33), within the margin of error, proving that our method accurately reproduces the literature values.[28] A decrease of the fluorescence quantum yield in solution under atmospheric conditions can be observed when changing the phenyl (Φ_f = 0.22) linker to

Table 3 Spectroscopic data for the three emitter molecules

Compound	λ_{abs} [a] (nm)	ε [b] (M^{-1} cm^{-1})	λ_{em} [c] (nm)	$\Phi_{f,atm,sol}$ [d]	$\Phi_{f,inert,sol}$ [e]	$\Phi_{f,atm,film}$ [f]	$\Phi_{f,inert,film}$ [g]	Φ_{Δ} [h]
BTaz-Ph-PXZ	308	25 900	479	0.22	0.35	0.12	0.48	0.33
	401	3 000						
BTaz-Na-PXZ	327	12 500	473	0.13	0.17	0.13	0.18	0.46
	405	3 000						
BTaz-Th-PXZ	323	11 500	481	0.02	0.03	0.09	0.11	0.59
	402	2700						

[a] Absorption maxima in toluene solution. [b] Molar extinction coefficients at the absorption maxima in toluene solution. [c] Fluorescence emission maxima in zeonex film. [d] Photoluminescence quantum yields in toluene solution under normal atmosphere determined *vs.* quinine (Φ_f = 0.58, λ_{exc} = 347 nm in 0.1 M H_2SO_4). [e] Fluorescence quantum yields in toluene solution under inert atmosphere determined *vs.* quinine (λ_{exc} = 347 nm). [f] Absolute PLQYs in zeonex using an integrating sphere in air at room temperature. [g] Absolute PLQYs in zeonex using an integrating sphere in inert atmosphere at room temperature. [h] Singlet oxygen quantum yields in toluene solution determined *vs.* coronene (Φ_{Δ} = 0.90, λ_{exc} = 325 nm in toluene) by monitoring the absorbance of 1,3-DPBF at 414 nm.

naphthyl (Φ_f = 0.13), while the fluorescence almost vanishes for the thienyl bridge (Φ_f = 0.02). When performing the same measurements under inert atmosphere, it is clear that the fluorescence quantum yield improves significantly for the phenyl and naphthyl linkers (to Φ_f = 0.35 and 0.17, respectively), whereas the value remains very low for the thienyl linker. This is a first indication that **BTaz-Ph-PXZ** and **BTaz-Na-PXZ** could benefit from some kind of triplet up-conversion mechanism as oxygen is no longer able to quench the intermittent triplet states in degassed solution. In zeonex film, the photoluminescence quantum yields (PLQYs) follow the same trend as in solution. The PLQYs are again lower in air than under inert atmosphere and the thienyl linked molecule has a lower PLQY than the phenyl and naphthyl counterparts. Since the zeonex

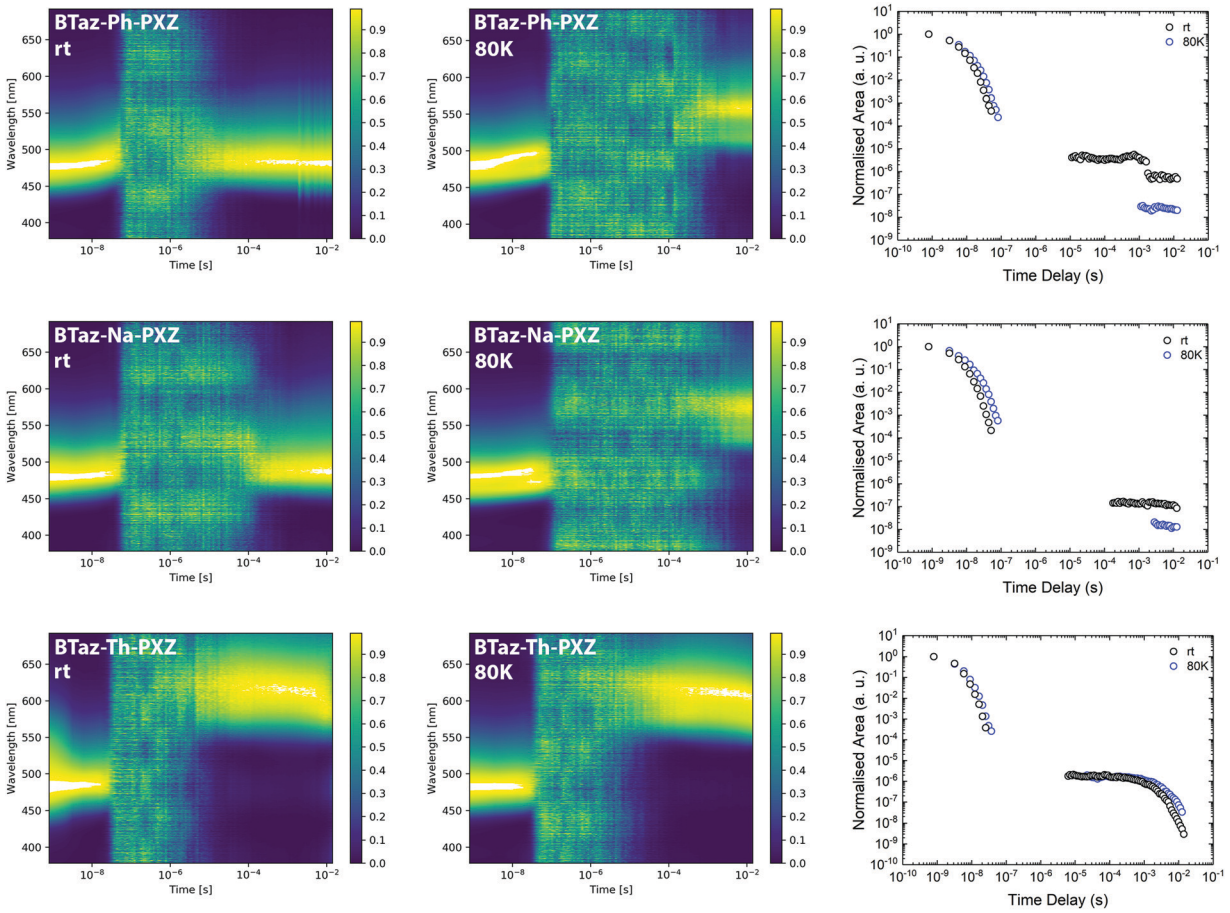

Fig. 3 Normalised time-resolved emission spectra for **BTaz-Ph-PXZ**, **BTaz-Na-PXZ**, and **BTaz-Th-PXZ** in zeonex at room temperature (left) and at 80 K (middle), and decay of the total emission for the three dyads in zeonex at room temperature (rt) and at 80 K (right). The noise arising between the prompt and delayed emission is coming from the CCD camera. The discontinuity in the room temperature decay of **BTaz-Ph-PXZ** at around 10^{-3} s is due to alteration of the laser settings during the decay measurement. Data points without signal have been omitted from the decay, but are retained in the contour plots.

matrix is a solid host, rotational and vibrational modes are more restricted and this is especially beneficial for **BTaz-Th-PXZ**, which seems to suffer from large non-radiative losses in solution. On the other hand, **BTaz-Ph-PXZ** seemingly fluoresces less in solid film as opposed to in toluene solution. The increases going from air to inert atmosphere are even more significant in zeonex film (Table 3).

Time-resolved emission spectroscopy (TRES) experiments in a zeonex host (at 1 w/w% loading), with a polarity similar to methylcyclohexane, were then performed to unravel the detailed emission mechanisms. The contour maps of the normalised TRES experiments for the three compounds at room temperature and at 80 K are shown in Fig. 3 (left and middle) and individual spectra extracted at different time intervals are provided in Fig. S8–S10 (ESI†). The prompt fluorescence, which vanishes within the first 100 ns, shows a small red-shift in the initial period, which is most pronounced for **BTaz-Ph-PXZ** and **BTaz-Na-PXZ**. This red-shift could be the result of a combination of emission from excited singlet states with slightly different molecular geometries, typically caused by different dihedral angles between the donor and acceptor unit. These differences in geometry will affect the radiative lifetime, ISC rate, *etc.* Afterwards, the emission falls below the detection limit of the detector until a time delay in the microseconds regime. Thereafter, delayed emission at room temperature occurs with the same energy as the prompt fluorescence in the case of **BTaz-Ph-PXZ** and **BTaz-Na-PXZ**. This suggests TADF or TTA to occur, as in both cases the delayed emission originates from the same emissive singlet state, and confirms our earlier hypothesis of a triplet up-conversion mechanism being at work. At 80 K, the delayed emission for both compounds is slightly red-shifted with respect to the prompt emission and can be attributed to phosphorescence. In contrast, the delayed emission for **BTaz-Th-PXZ** at room temperature is already strongly red-shifted compared to the prompt fluorescence and the contour maps of the TRES experiments recorded at room temperature and 80 K (Fig. 3, left and middle) are almost identical. This is further supported by looking at the individual emission spectra obtained at various time delays during the emission decays. The emission spectrum for the phosphorescence of **BTaz-Th-PXZ** is similar to the spectra of its delayed emission at room temperature (Fig. S9, ESI†). Therefore, we can conclude that the delayed emission of **BTaz-Th-PXZ** is due to RTP. The latter is also visible in the steady-state emission spectrum under inert atmosphere (Fig. S11, ESI†).

To distinguish between TADF and TTA as the delayed emission mechanism for **BTaz-Ph-PXZ** and **BTaz-Na-PXZ**, laser energy experiments were performed (Fig. S12, ESI†). The dependence of emission intensity on excitation laser energy was measured by attenuation of the excitation beam with reflective neutral density filters. Throughout the entire experiment, the slope of the log–log plot remained unity, suggesting TADF as the emission mechanism in both cases. Moreover, **BTaz-Th-PXZ** also showed a slope of $\sim$1, confirming RTP emission.

The emission decays for all three compounds, presented as the normalised integrated area *versus* time at room temperature and at 80 K (Fig. 3, right), give more insight into the kinetics of the emission. All compounds show prompt emission at room temperature and at 80 K, with a nanoseconds lifetime (Table 4). A relatively long-lived and intense delayed emission is seen for **BTaz-Ph-PXZ** and **BTaz-Na-PXZ** at room temperature. At 80 K, the lower intensity and longer timescale of the emission is due to the disappearance of the delayed emission and appearance of phosphorescence, confirming a temperature dependent mechanism such as TADF. In the case of **BTaz-Th-PXZ**, the decay of the total emission at room temperature and at 80 K is nearly identical, confirming RTP. The lifetimes of the prompt and delayed components in zeonex have been obtained *via* biexponential fitting of the decay curves (Table 4). While **BTaz-Ph-PXZ** and **BTaz-Na-PXZ** have similar lifetimes for the prompt fluorescence, **BTaz-Th-PXZ** has a clearly shorter lifetime. The lifetimes of the delayed components in zeonex are very large, indicating that rISC is not very efficient in these materials.

Table 4 Lifetimes of the prompt and delayed emission components at room temperature as determined from the TRES experiments

Compound	Sample	τ_{prompt}[a] (ns)	$\tau_{delayed}$[a] (μs)
BTaz-Ph-PXZ	Zeonex	4.7	–[b]
	Toluene	13.7	143.7
	Chloroform	9.1	5.2
BTaz-Na-PXZ	Zeonex	4.6	–[b]
	Toluene	6.2	64.8
	Chloroform	10.2	15.8
BTaz-Th-PXZ	Zeonex	2.8	1.5×10^3
	Toluene	2.6	106.6
	Chloroform	2.4	33.2

[a] Lifetime of the emission as obtained using a biexponential fit. A weighted average of the two lifetimes was made. [b] Accurate lifetimes cannot be determined.

With the information from the time-resolved emission at 80 K (phosphorescence) and the steady-state emission spectra in zeonex (Fig. 2), it is possible to determine the triplet and singlet energy, respectively, by looking at the onset of the emission (Table 5). As expected from the theoretical calculations, the singlet energies are comparable for all three compounds. However, a significant decrease is observed for the triplet energy within the series, from 2.55 eV (phenyl) to 2.34 eV (thienyl). As the $S_0 \rightarrow T_1$ vertical excitation is mostly located on the BTaz-π-linker part of the molecule (Fig. S1, ESI†), it makes sense that the experimental triplet energy is most influenced by the structural changes. The increased delocalization for the naphthyl with respect to the phenyl linker stabilises the triplet state energy and the heteroaromatic thiophene seemingly has an even larger

Table 5 Singlet and triplet energies derived from the steady-state and time-resolved emission spectra in 1 w/w% zeonex films, respectively

Compound	E_S (eV)[a]	E_T (eV)[b]	ΔE_{ST} (eV)[c]
BTaz-Ph-PXZ	2.85	2.55	0.30
BTaz-Na-PXZ	2.83	2.46	0.37
BTaz-Th-PXZ	2.83	2.34	0.49

[a] Taken from the onset of the steady-state emission in zeonex film. [b] Taken from the onset of the phosphorescence emission at ms time-scales at 80 K in zeonex film. [c] Calculated as $E_S - E_T$.

stabilizing effect. As a result, the experimental singlet–triplet energy splitting increases upon moving from **BTaz-Ph-PXZ** to **BTaz-Th-PXZ**. The theoretical calculations predicted **BTaz-Na-PXZ** to have the largest ΔE_{ST} and this discrepancy with respect to the experimental results can be related to the way the singlet–triplet gap is determined, *i.e. via* the difference between two vertical excitation energies for TDDFT or *via* the onset of the prompt fluorescence and phosphorescence for the experimental results. While these experimental singlet–triplet splittings are relatively large for **BTaz-Ph-PXZ** (0.30 eV) and **BTaz-Na-PXZ** (0.37 eV), they make the thermal up-conversion (rISC) difficult, but not impossible.[23] For **BTaz-Th-PXZ**, on the other hand, the ΔE_{ST} (0.49 eV) is too large for rISC to occur and therefore the radiative transition from the triplet excited state to the singlet ground state becomes plausible.

To get a deeper understanding of the photophysical properties of the three compounds in solution, and more particular **BTaz-Th-PXZ**, TRES experiments were performed in degassed toluene (ε = 2.38) and chloroform (ε = 4.81) at a concentration of 50 μM. The contour maps and the decay plots of **BTaz-Ph-PXZ** measured at room temperature in these two solvents are shown in Fig. S13 (ESI†). In both cases, the contour plots clearly show delayed emission originating from the same excited state as the prompt fluorescence, suggesting TADF. The polarity of the solvent, however, does have an effect on the emission wavelength as **BTaz-Ph-PXZ** emits at 530 nm in toluene, whereas it emits at 575 nm in chloroform, implying strong excited state stabilisation in more polar environments. Consistent with the solid-state measurements, **BTaz-Na-PXZ** shows similar properties as **BTaz-Ph-PXZ**, as shown in Fig. S14 (ESI†). The contour maps and decay plots in toluene and chloroform also show TADF in both solvents for **BTaz-Na-PXZ**, albeit a bit less intense than for **BTaz-Ph-PXZ**. The thienyl variant **BTaz-Th-PXZ** shows relatively intense delayed emission in solution, with reasonably long lifetimes of 33.2 μs and 106.6 μs in chloroform and toluene, respectively (Table 4). Strongly red-shifted with respect to the prompt fluorescence (Fig. 4 and Fig. S15, ESI†) and similar to its behaviour in zeonex, this is assigned to RTP. This is somewhat surprising as phosphorescence at room temperature in solution has only rarely been observed for halogen-free purely organic compounds due to the strong competition between the typically slow phosphorescence and the relatively fast non-radiative decay pathways (collisional quenching and internal conversion). We note, however, that the relatively low solution PLQYs (both with and without the presence of oxygen, Table 3) indicate quenching processes are still strongly active, and the RTP we do observe originates only from the small population of molecules for which triplet emission outcompetes quenching.

Since we observe TADF for the phenyl and naphthyl linked compounds and RTP for the thienyl bridged material, triplet excited states play a crucial role in the (time-resolved) photophysics of these materials. Independent of the exact emission process, molecular oxygen can lead to quenching of excited triplet states to undergo a transition from its triplet ground state to the singlet excited state ($^3O_2 + T_n \rightarrow {}^1O_2 + S_0$). Singlet oxygen formation can thus be used as an indirect method to prove triplet formation in photosensitizers.[46] This is also at the origin of the difference in PLQY in air and under inert atmosphere for compounds showing triplet up-conversion or triplet emission. Singlet oxygen quantum yields (Φ_Δ, Table 3)

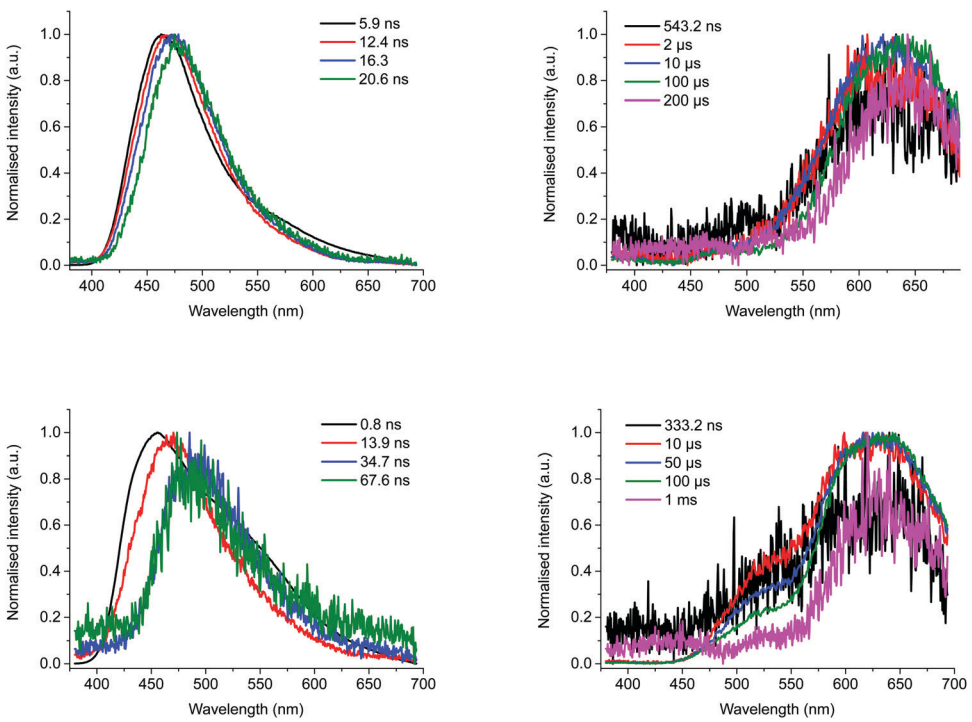

Fig. 4 Snapshots of the emission at various time scales during prompt (left) and delayed emission (right) for **BTaz-Th-PXZ** at room temperature in chloroform (top) and in toluene (bottom) solution.

were measured using a relative method in which the reaction of a $^1O_2$ scavenger (1,3-diphenylisobenzofuran, 1,3-DPBF) is monitored *via* UV-Vis absorption spectroscopy while the photosensitizer (*i.e.* the BTaz compound) is illuminated using a secondary light source (Fig. S16, ESI†). The singlet oxygen quantum yields follow the opposite trend of the PLQYs, with **BTaz-Th-PXZ** (Φ_Δ = 0.59) showing the largest value, followed by **BTaz-Na-PXZ** (Φ_Δ = 0.46) and **BTaz-Ph-PXZ** (Φ_Δ = 0.33).

These values, in combination with the PLQYs under inert atmosphere, can be rationalised by looking at the experimental singlet–triplet splittings of these materials (Table 5). The phenyl and naphthyl linked molecules both show TADF, so transitions from the triplet state to the ground state are in competition with the rISC pathway. The phenyl bridged molecule has a smaller ΔE_{ST}, which means that the rISC rate will be higher and thus the singlet oxygen quantum yield will be lower than that of **BTaz-Na-PXZ**. **BTaz-Th-PXZ** shows RTP, which means that the transitions from the triplet excited state are in competition with radiative relaxation to the ground state. This is a spin-forbidden process and combined with the low PLQY, a large amount of triplet excitons are required to see the phosphorescence. Due to its large ΔE_{ST}, the rISC pathway is not viable for this molecule and the triplet excitons are trapped until (non-)radiative decay allows them to relax back to the ground state. The results can also be interpreted in terms of the ISC rate. While it is not straightforward to derive the ISC rate from the emission decays, the $^1O_2$ quantum yields show that ISC is most efficient in **BTaz-Th-PXZ** when compared to **BTaz-Na-PXZ** and **BTaz-Ph-PXZ**.

As mentioned before, the singlet oxygen quantum yields are related to the ISC and, when applicable, rISC rates. Apart from the energy difference between the involved excited states, the spin–orbit coupling between them also plays a crucial role. For **BTaz-Ph-PXZ**, the $T_1 \rightarrow S_0$ transition has a large SOC value in comparison to the other two compounds (Fig. 5). It must be noted that for **BTaz-Ph-PXZ** the first excited triplet state has significant CT character and the second excited triplet state has LE character, whereas the inverse is true for **BTaz-Na-PXZ** and **BTaz-Th-PXZ** (Table 2 and Fig. 5). Therefore, we need to compare this value with the $T_2 \rightarrow S_0$ transition for the naphthyl and thienyl linked compounds. Indeed, in comparison with the LE triplet states, the triplet states with CT character have the largest SOC value for the transition to S_0. For **BTaz-Ph-PXZ**, the rISC pathway is likely outcompeting the radiative triplet decay to the ground state due to the higher-lying triplet state and smaller ΔE_{ST}. For **BTaz-Na-PXZ**, the SOC values for both the $T_1/T_2 \rightarrow S_0$ transitions are small and these are therefore unlikely to occur.

BTaz-Th-PXZ has a very large SOC value for the $T_2 \rightarrow S_0$ transition and the T_1–T_2 energy splitting is only 0.07 eV, making vibronic mixing between these two states possible. The aforementioned, in combination with the relatively large ΔE_{ST}, is likely giving rise to the RTP that we observe in the TRES experiments. To enable rISC between excited states of different multiplicities, vibrational mixing of the CT and LE triplet states is required and this is plausible because of the small energy difference (0.07 eV, Table 1) between the two states. For the ISC pathway, the $S_1 \rightarrow T_1$ and $S_1 \rightarrow T_2$ transitions are investigated. Since the S_1 state is of CT character for all compounds, according to the El Sayed rule,[47] we expect the largest SOC values to be found for the CT→LE transition, which corresponds to the $S_1 \rightarrow T_2$ transition for **BTaz-Ph-PXZ** and to the $S_1 \rightarrow T_1$ transition for **BTaz-Na-PXZ** and **BTaz-Th-PXZ**. The phenyl linked molecule has a slightly higher SOC value than the naphthyl linked molecule for the CT→LE transition, but T_2 is also higher in energy than S_1 for **BTaz-Ph-PXZ**, whereas both T_2 and T_1 are lower in energy than S_1 for **BTaz-Na-PXZ** (Fig. 5). Therefore, the $S_1 \rightarrow T_2$ ISC transition is not available for **BTaz-Ph-PXZ** and this could explain why the naphthyl variant has a higher triplet formation yield. **BTaz-Th-PXZ** has the highest SOC value for the ISC process, as is also reflected in the singlet oxygen quantum yields. Heavy atoms, such as sulfur, are known to afford stronger SOC effects, leading to higher ISC rates, and thereby increasing the chance for RTP to occur.[48–54] In addition,

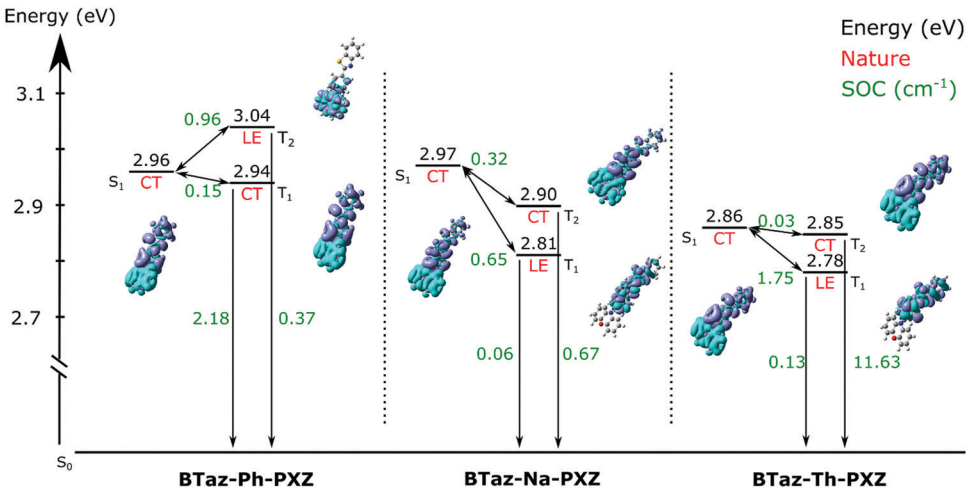

Fig. 5 Schematic representation of the ground and excited state energy levels with their corresponding CT/LE character and the spin–orbit coupling values (in cm^{-1}) between these various excited states as obtained using TDDFT calculations with LC-BLYP (ω = 0.17 $bohr^{-1}$)/6-311G(d) under the TDA and applying the PCM (cyclohexane).

the ground and excited state energy difference densities (Fig. 5 and Fig. S1, ESI†) show that the thiophene unit is involved in all transitions under investigation for **BTaz-Th-PXZ**, increasing the influence of the central sulfur atom on the SOC values. These results indicate that the thienyl linker imposes a significantly higher tendency to give ISC.

Conclusions

In this work, we presented the design and synthesis of three small molecule benzothiazole-π-bridge-phenoxazine emitters, each with a different aromatic bridging moiety. An extended photophysical study was performed, both in solution and in zeonex film. The fluorescence quantum yield goes down when changing the phenyl bridge to naphthyl and even further to thienyl, whereas the opposite is true for the ability to generate singlet oxygen. The emission mechanism, first in the solid state, was studied using time-resolved emission spectroscopy by doping the emitters in a zeonex matrix. These measurements showed that the emission wavelength is similar for all three dyads, although they possess different triplet energies. Consequently, thermally activated delayed fluorescence was seen for **BTaz-Ph-PXZ** and (somewhat weaker) for **BTaz-Na-PXZ**, whereas room temperature phosphorescence was noticed for **BTaz-Th-PXZ**, even in solution. The observation of phosphorescence in solution correlates with the high singlet oxygen generation and possibly opens up applications in other fields such as (image-guided) photodynamic therapy.[55–57] Altering the π-bridge thus has a drastic effect on the excited/ground-state transition rates governing the emission mechanism, which consequently has a significant impact on the photophysical properties. These results provide further insights into the relationship between the bridging moiety and the photophysical properties of D-π-A type small-molecule emitters and contribute to the future development of applications relying on different types of emission from purely organic molecules.

Conflicts of interest

There are no conflicts to declare.

Acknowledgements

The authors thank the Research Foundation – Flanders (FWO Vlaanderen) for financial support (projects G087718N, G0D1521N, I006320N, GOH3816NAUHL, the Scientific Research Community 'Supramolecular Chemistry and Materials' (W000620N), and PhD scholarship S. Paredis). The calculations were performed on the computers of the 'Consortium des équipements de Calcul Intensif (CÉCI)' (http://www.ceci-hpc.be), including those of the 'UNamur Technological Platform of High-Performance Computing (PTCI)' (http://www.ptci.unamur.be), for which we gratefully acknowledge the financial support from the FNRS-FRFC, the Walloon Region, and the University of Namur (Conventions No. 2.5020.11, GEQ U.G006.15, U.G018.19, 1610468, and RW/GEQ2016). A. Danos and A. P. Monkman are supported by EU Horizon 2020 Grant Agreement No. 732013 (HyperOLED) and EPSRC grant EP/T02240X/1.

References

1 J. Kalinowski, in *Electrical and Related Properties of Organic Solids*, Springer, Netherlands, Dordrecht, 1997, pp. 167–206.
2 L. Wang, L. Xiao, H. Gu and H. Sun, *Adv. Opt. Mater.*, 2019, **7**, 1801154.
3 M. R. Narayan and J. Singh, in *Excitonic and Photonic Processes in Materials*, ed. J. Singh, R. T. Williams, Springer, 2015, pp. 229–251.
4 M. Segal, M. A. Baldo, R. J. Holmes, S. R. Forrest and Z. G. Soos, *Phys. Rev. B: Condens. Matter Mater. Phys.*, 2003, **68**, 075211.
5 T. Tsujimura, *OLED Display Fundamentals and Applications*, John Wiley & Sons, Inc., Hoboken, New Jersey, 2017.
6 D. T. Yonemoto, C. M. Papa, C. Mongin and F. N. Castellano, *J. Am. Chem. Soc.*, 2020, **142**, 10883–10893.
7 R. Chen, Y. Tang, Y. Wan, T. Chen, C. Zheng, Y. Qi, Y. Cheng and W. Huang, *Sci. Rep.*, 2017, **7**, 6225.
8 Z. Yang, Z. Mao, Z. Xie, Y. Zhang, S. Liu, J. Zhao, J. Xu, Z. Chi and M. P. Aldred, *Chem. Soc. Rev.*, 2017, **46**, 915–1016.
9 Y. Tao, K. Yuan, T. Chen, P. Xu, H. Li, R. Chen, C. Zheng, L. Zhang and W. Huang, *Adv. Mater.*, 2014, **26**, 7931–7958.
10 X. Liang, Z. Tu and Y. Zheng, *Chem. – Eur. J.*, 2019, **25**, 5623–5642.
11 L. B. McGown and K. Nithipatikom, *Appl. Spectrosc. Rev.*, 2000, **35**, 353–393.
12 J. Gibson, A. P. Monkman and T. J. Penfold, *Chem. Phys. Chem.*, 2016, **17**, 2956–2961.
13 P. Data and Y. Takeda, *Chem. – Asian J.*, 2019, **14**, 1613–1636.
14 Q. Wei, N. Fei, A. Islam, T. Lei, L. Hong, R. Peng, X. Fan, L. Chen, P. Gao and Z. Ge, *Adv. Opt. Mater.*, 2018, **6**, 1800512.
15 N. A. Kukhta and M. R. Bryce, *Mater. Horiz.*, 2021, **8**, 33–55.
16 Z. An, C. Zheng, Y. Tao, R. Chen, H. Shi, T. Chen, Z. Wang, H. Li, R. Deng, X. Liu and W. Huang, *Nat. Mater.*, 2015, **14**, 685–690.
17 L. Gu, H. Shi, L. Bian, M. Gu, K. Ling, X. Wang, H. Ma, S. Cai, W. Ning, L. Fu, H. Wang, S. Wang, Y. Gao, W. Yao, F. Huo, Y. Tao, Z. An, X. Liu and W. Huang, *Nat. Photonics*, 2019, **13**, 406–411.
18 J. Xu, A. Takai, Y. Kobayashi and M. Takeuchi, *Chem. Commun.*, 2013, **49**, 8447.
19 B. Ventura, A. Bertocco, D. Braga, L. Catalano, S. D'Agostino, F. Grepioni and P. Taddei, *J. Phys. Chem. C*, 2014, **118**, 18646–18658.
20 Q. Zhang, H. Kuwabara, W. J. Potscavage, S. Huang, Y. Hatae, T. Shibata and C. Adachi, *J. Am. Chem. Soc.*, 2014, **136**, 18070–18081.
21 W. Wei, Z. Yang, X. Chen, T. Liu, Z. Mao, J. Zhao and Z. Chi, *J. Mater. Chem. C*, 2020, **8**, 3663–3668.
22 P. Stachelek, J. S. Ward, P. L. dos Santos, A. Danos, M. Colella, N. Haase, S. J. Raynes, A. S. Batsanov,

M. R. Bryce and A. P. Monkman, *ACS Appl. Mater. Interfaces*, 2019, **11**, 27125–27133.
23 J. S. Ward, A. Danos, P. Stachelek, M. A. Fox, A. S. Batsanov, A. P. Monkman and M. R. Bryce, *Mater. Chem. Front.*, 2020, **4**, 3602–3615.
24 H. L. Lee, K. H. Lee, J. Y. Lee and W. P. Hong, *J. Mater. Chem. C*, 2019, **7**, 6465–6474.
25 K. H. Lee, S. O. Jeon, Y. S. Chung, M. Numata, H. Lee, E. K. Lee, E. S. Kwon, M. Sim, H. Choi and J. Y. Lee, *J. Mater. Chem. C*, 2020, **8**, 1736–1745.
26 L. Xue, B. Cui, S. Xie and S. Yin, *J. Phys. Chem. Lett.*, 2019, **10**, 302–308.
27 Y. Gao, Y. Geng, Y. Wu, M. Zhang and Z.-M. Su, *Dyes Pigm.*, 2017, **145**, 277–284.
28 Y. Sagara, K. Shizu, H. Tanaka, H. Miyazaki, K. Goushi, H. Kaji and C. Adachi, *Chem. Lett.*, 2015, **44**, 360–362.
29 L. Mohammad, Q. Chen, A. Mitul, J. Sun, D. Khatiwada, B. Vaagensmith, C. Zhang, J. Li and Q. Qiao, *J. Phys. Chem. C*, 2015, **119**, 18992–19000.
30 G. K. Dutta, S. Guha and S. Patil, *Org. Electron.*, 2010, **11**, 1–9.
31 Y. Wang and T. Michinobu, *J. Mater. Chem. C*, 2016, **4**, 6200–6214.
32 A. Mabrouk, A. Azazi and K. Alimi, *J. Phys. Chem. Solids*, 2010, **71**, 1225–1235.
33 F. Li, M. Li, J. Fan, Y. Song, C.-K. Wang and L. Lin, *J. Phys. Chem. A*, 2020, **124**, 7526–7537.
34 W. Che, Y. Xie and Z. Li, *Asian J. Org. Chem.*, 2020, **9**, 1262–1276.
35 B. Sk, S. Sharma, A. James, S. Kundu and A. Patra, *J. Mater. Chem. C*, 2020, **8**, 12943–12950.
36 A. A. Weekes, M. C. Dix, M. C. Bagley and A. D. Westwell, *Synth. Commun.*, 2010, **40**, 3027–3032.
37 Y. Zhao and D. G. Truhlar, *Theor. Chem. Acc.*, 2008, **120**, 215–241.
38 T. J. Penfold, *J. Phys. Chem. C*, 2015, **119**, 13535–13544.
39 T. Cardeynaels, S. Paredis, J. Deckers, S. Brebels, D. Vanderzande, W. Maes and B. Champagne, *Phys. Chem. Chem. Phys.*, 2020, **22**, 16387–16399.
40 M. J. Frisch, G. W. Trucks, H. B. Schlegel, G. E. Scuseria, M. A. Robb, J. R. Cheeseman, G. Scalmani, V. Barone, G. A. Petersson, H. Nakatsuji, X. Li, M. Caricato, A. V. Marenich, J. Bloino, B. G. Janesko, R. Gomperts, B. Mennucci, H. P. Hratchian, J. V. Ortiz, A. F. Izmaylov, J. L. Sonnenberg, D. Williams-Young, F. Ding, F. Lipparini, F. Egidi, J. Goings, B. Peng, A. Petrone, T. Henderson, D. Ranasinghe, V. G. Zakrzewski, J. Gao, N. Rega, G. Zheng, W. Liang, M. Hada, M. Ehara, K. Toyota, R. Fukuda, J. Hasegawa, M. Ishida, T. Nakajima, Y. Honda, O. Kitao, H. Nakai, T. Vreven, K. Throssell, J. A. Montgomery Jr., J. E. Peralta, F. Ogliaro, M. J. Bearpark, J. J. Heyd, E. N. Brothers, K. N. Kudin, V. N. Staroverov, T. A. Keith, R. Kobayashi, J. Normand, K. Raghavachari, A. P. Rendell, J. C. Burant, S. S. Iyengar, J. Tomasi, M. Cossi, J. M. Millam, M. Klene, C. Adamo, R. Cammi, J. W. Ochterski, R. L. Martin, K. Morokuma, O. Farkas, J. B. Foresman and D. J. Fox, *Gaussian 16, revision A.03*, Gaussian, Inc., Wallingford CT, 2016.
41 T. Le Bahers, C. Adamo and I. Ciofini, *J. Chem. Theory Comput.*, 2011, **7**, 2498–2506.
42 X. Gao, S. Bai, D. Fazzi, T. Niehaus, M. Barbatti and W. Thiel, *J. Chem. Theory Comput.*, 2017, **13**, 515–524.
43 K. Wang, C.-J. Zheng, W. Liu, K. Liang, Y.-Z. Shi, S.-L. Tao, C.-S. Lee, X.-M. Ou and X.-H. Zhang, *Adv. Mater.*, 2017, **29**, 1701476.
44 E. Borowska, E. Felis and J. Kalka, *Chem. Eng. J.*, 2016, **304**, 852–863.
45 X. Han, X. Zhang, L. Zhang, M. Pan and J. Yan, *R. Soc. Open Sci.*, 2018, **5**, 180322.
46 J. R. Kanofsky, in *Singlet Oxygen: Applications in Biosciences and Nanosciences*, 2016, Volume 1, p. 11.
47 M. A. El-Sayed, *J. Chem. Phys.*, 1963, **38**, 2834–2838.
48 J. Deckers, T. Cardeynaels, L. Lutsen, B. Champagne and W. Maes, *ChemPhysChem*, 2021, **22**, 1488–1496.
49 T. Cardeynaels, S. Paredis, A. Danos, D. Vanderzande, A. P. Monkman, B. Champagne and W. Maes, *Dyes Pigm.*, 2021, **186**, 109022.
50 T. Cardeynaels, S. Paredis, A. Danos, A. Harrison, J. Deckers, S. Brebels, L. Lutsen, D. Vanderzande, A. P. Monkman, B. Champagne and W. Maes, *Dyes Pigm.*, 2021, **190**, 109301.
51 S. Hirata, *Adv. Opt. Mater.*, 2017, **5**, 1700116.
52 P. Pander, A. Swist, R. Motyka, J. Soloducho, F. B. Dias and P. Data, *J. Mater. Chem. C*, 2018, **6**, 5434–5443.
53 N. A. Kukhta, R. Huang, A. S. Batsanov, M. R. Bryce and F. B. Dias, *J. Phys. Chem. C*, 2019, **123**, 26536–26546.
54 J. S. Ward, R. S. Nobuyasu, A. S. Batsanov, P. Data, A. P. Monkman, F. B. Dias and M. R. Bryce, *Chem. Commun.*, 2016, **52**, 2612–2615.
55 R. R. Allison, G. H. Downie, R. Cuenca, X.-H. Hu, C. J. Childs and C. H. Sibata, *Photodiagn. Photodyn. Ther.*, 2004, **1**, 27–42.
56 J. P. Celli, B. Q. Spring, I. Rizvi, C. L. Evans, K. S. Samkoe, S. Verma, B. W. Pogue and T. Hasan, *Chem. Rev.*, 2010, **110**, 2795–2838.
57 J. Deckers, T. Cardeynaels, H. Penxten, A. Ethirajan, M. Ameloot, M. Kruk, B. Champagne and W. Maes, *Chem. – Eur. J.*, 2020, **26**, 15212–15225.

